Orbital-scale climate forcing of grassland burning in southern Africa

Anne-Laure Daniau[a,b,c,1], Maria Fernanda Sánchez Goñi[b], Philippe Martinez[a], Dunia H. Urrego[a,b,c], Viviane Bout-Roumazeilles[d], Stéphanie Desprat[b], and Jennifer R. Marlon[e]

[a]Centre National de la Recherche Scientifique (CNRS), Environnements et Paléoenvironnements Océaniques et Continentaux (EPOC), Unité Mixte de Recherche (UMR) 5805, Université Bordeaux 1, F-33400 Talence, France; [b]Ecole Pratique des Hautes Etudes (EPHE), EPOC, UMR 5805, F-33400 Talence, France; and [c]CNRS, de la Préhistoire à l'Actuel: Culture, Environnement et Anthropologie (PACEA), UMR 5199, F-33400 Talence, France; [d]Géosystèmes UMR 8217 CNRS, Sciences de la Terre, Université Lille 1, 59655 Villeneuve d'Ascq, France; and [e]School of Forestry and Environmental Studies, Yale University, New Haven, CT 06511

Edited by William F. Ruddiman, University of Virginia, Charlottesville, VA, and accepted by the Editorial Board February 12, 2013 (received for review August 17, 2012)

Although grassland and savanna occupy only a quarter of the world's vegetation, burning in these ecosystems accounts for roughly half the global carbon emissions from fire. However, the processes that govern changes in grassland burning are poorly understood, particularly on time scales beyond satellite records. We analyzed microcharcoal, sediments, and geochemistry in a high-resolution marine sediment core off Namibia to identify the processes that have controlled biomass burning in southern African grassland ecosystems under large, multimillennial-scale climate changes. Six fire cycles occurred during the past 170,000 y in southern Africa that correspond both in timing and magnitude to the precessional forcing of north–south shifts in the Intertropical Convergence Zone. Contrary to the conventional expectation that fire increases with higher temperatures and increased drought, we found that wetter and cooler climates cause increased burning in the study region, owing to a shift in rainfall amount and seasonality (and thus vegetation flammability). We also show that charcoal morphology (i.e., the particle's length-to-width ratio) can be used to reconstruct changes in fire activity as well as biome shifts over time. Our results provide essential context for understanding current and future grassland-fire dynamics and their associated carbon emissions.

Large changes in the spatiotemporal patterns of wildfires in recent decades raise concerns about how future changes in fire might interact with climate change and human activities (1, 2). Africa is the most fire-prone continent, and southern Africa is recognized as a climate change and biodiversity hotspot (3, 4). Under global warming, fire risk is projected to increase by the end of the 21st century in this region owing to a rise in temperatures and austral winter dryness (5, 6). Projected wildfires, however, vary substantially depending on the general circulation model (GCMs) and Intergovernmental Panel on Climate Change (IPCC) emission scenarios used (6). GCMs seldom take into account vegetation adjustments to climate changes, yet such changes are vital for projecting reliable shifts in fuels and thus fire activity (6). Under increased aridity, for example, longer or more frequent droughts may promote burning in ecosystems that are not fuel limited. However, vegetation shifts toward fuel-limited communities may reduce fire activity in the same region (7, 8).

Currently there are no empirical data to support the idea that a warming and drying climate would lead to an increase in biomass burning in southern Africa. In fact, a number of remotely sensed data indicate that wetter periods result in increased fire in this region (8–10). To address this question, we examined microcharcoal from a marine sediment record that accumulated during the past two climatic cycles off southwestern Africa and covers several past warm periods. We analyzed the sediment to confirm that variations in microcharcoal concentrations reflect biomass burning rather than transportation or depositional processes. We then compared the fire data with orbital parameters, rainfall, and vegetation changes to identify the primary controls on biomass burning over the past 170,000 y.

There are two major types of fire-prone vegetation in southern Africa: eastern grasslands and southwestern fynbos (Mediterranean evergreen hard-leaved scrub). Fire is absent from the desert and semidesert regions (Fig. 1). The eastern half of southern Africa and the northern Cape regions, Namibia, and Botswana are dominated by arid savanna and grasslands that support surface fires (9) (Fig. 1). These regions are under the influence of the Intertropical Convergence Zone (ITCZ), and their climatic regime is modulated by the South African monsoon, which brings rainfall during the austral summer (November–March) (11). Surface fires occur mainly during the peak of the dry season from July to September (austral winter) and are highly dependent on the accumulated rainfall of the previous 2 y (which drives fuel loads), as well as on marked rainfall seasonality (i.e., a limited number of months with rainfall) (9). In general, the seasonality causes fuel build-up during the wet austral summers and increased fuel flammability during dry winters. Ignitions in the region come from both lightning and humans today, but lightning alone would provide an ample source of ignitions for fires even in the absence of humans (12).

In the southern and southwestern regions (western Cape), winter-rainfall fynbos provide woody fuels that support crown fires during the dry season of the western Cape (i.e., from December to February), corresponding to the wet austral summer period when precipitation mainly falls in the eastern part of southern Africa. These fires burn dense sclerophyllous shrubs and small trees. They are most likely to occur after exceptional weather conditions, especially prolonged drought (9, 13, 14). Large fires are common in savanna and grassland, but increasingly fragmented vegetation induced by human activities reduces landscape connectivity and wildfire occurrences in these vegetation types (15).

Results and Discussion

Microcharcoal belongs to the fine sediment fraction and is transported by winds and river plumes from southern African combustion sites to the Atlantic Ocean. The main source of microcharcoal is not well constrained but is very likely limited to southern Africa below 20°S. The Orange River's hydrographic

Author contributions: A.-L.D. and M.F.S.G. designed research; A.-L.D. performed research; A.-L.D., P.M., and V.B.-R. contributed new reagents/analytic tools; A.-L.D., M.F.S.G., P.M., D.H.U., V.B.-R., S.D., and J.R.M. analyzed data; and A.-L.D., M.F.S.G., P.M., D.H.U., V.B.-R., S.D., and J.R.M. wrote the paper.

The authors declare no conflict of interest.

This article is a PNAS Direct Submission. W.F.R. is a guest editor invited by the Editorial Board.

[1]To whom correspondence should be addressed. E-mail: al.daniau@epoc.u-bordeaux1.fr.

This article contains supporting information online at www.pnas.org/lookup/suppl/doi:10.1073/pnas.1214292110/-/DCSupplemental.

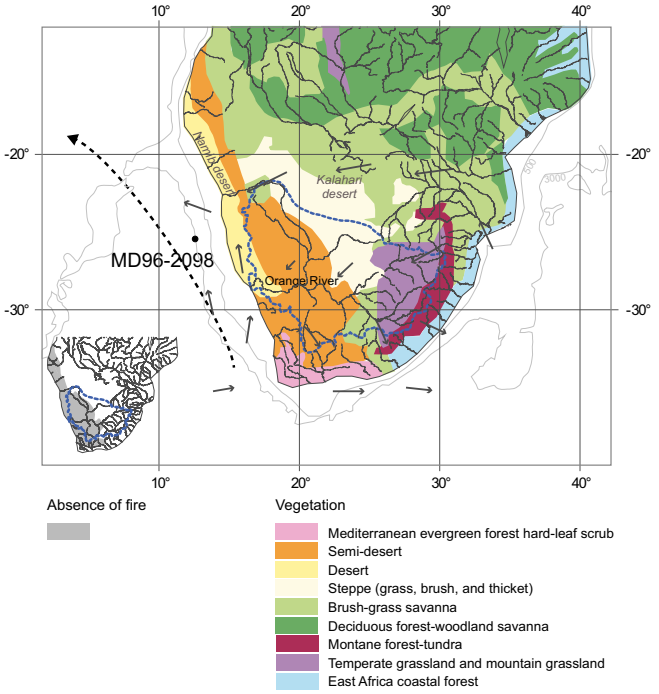

Fig. 1. Map of southern Africa with the location of marine core MD96-2098, the Orange River's hydrographic basin (dashed blue line), and simplified vegetation distribution, after ref. 48. Arrows indicate mean annual wind direction (redrawn from National Centers for Environmental Prediction/National Center for Atmospheric Research (NCEP/NCAR) reanalysis, mean annual 850-mb vector wind calculated over 1948–2012, www.esrl.noaa.gov/psd/). Black dashed arrow indicates the Benguela current (17). Bathymetric data extracted from the General Bathymetric Chart of the Oceans (GEBCO; www.gebco.net). (*Inset*) Gray color indicates areas characterized by absence of fire, after ref. 9.

basin is the largest river catchment area in southern Africa (Fig. 1). The annual water discharge of the Orange River is relatively low, but the annual suspended sediment flux is the highest among other African rivers (16). Easterly winds are dominant and blow over southern Africa throughout the year (11) (Fig. 1). The Southeast Trade Winds are perennially consistent between 22°S and 27°S (17). The present-day circulation of the southeast Atlantic upper waters along the southwestern African margin is associated with the northward flow of the Benguela Current (Fig. 1) (17), which represents a potential carrier of sediments from southern Africa to the core location. The studied site has been under the influence of this current at least for the last 500 ka (18–21). In addition, the present-day source of silicoclastic sediment in core MD96-2098 mainly consists of Namibian dust and southwestern Atlantic clays (<20% Congo river clay input) (22). During glacial times, the Congo River's material contribution to the core location was reduced from ~20% to ~10% (22). Consequently, the source area for microcharcoal particles in the core is very likely limited to southern Africa, even during glacial times.

Variations of microcharcoal concentrations (CCnb, Fig. 2*F*) form six cycles, with alternating peaks at approximately 41, 70, 97, 116, 136, and 160 ka (ky cal BP) and troughs at 53, 78, 103, 124, and 146 ka. We normalized microcharcoal concentrations with Ca_{XRF} and $(Al+K+Ti+Fe)_{XRF}$ content (Fig. 2*A*) to evaluate whether they are affected by dilution of biogenic or terrigenous material, respectively (Fig. 2 *B* and *C* and Figs. S1 and S2). Normalized microcharcoal concentrations display the same variability pattern (frequency and amplitude) as the unnormalized microcharcoal concentrations, suggesting that dilution processes from either biogenic or terrigenous material do not significantly control microcharcoal concentrations variability. Today the Orange River is the primary source of smectite and kaolinite (23), whereas illite is transported by winds (23) toward the oceanic region where MD96-2098 was retrieved. Clay analyses (Fig. 2*D*) show that similar illite/smectite ratios are either associated with peaks or troughs of microcharcoal concentration (i.e., microcharcoal concentration variation is independent of changes in wind transport or river supply). As a result, variations in microcharcoal concentrations seem to reflect microcharcoal production and henceforth are interpreted as faithful records of changes in biomass burning and fire activity in southern Africa.

The morphometric analysis showed that more elongated particles are prevalent during periods of high fire activity. The mean elongation ratio is approximately 1.82 for high fire activity compared with approximately 1.65 for low activity (Fig. 2*E*, CCnb vs. elongation ratio, $r = 0.4$, $P < 0.001$). More elongated particles are found also during precession maxima (elongation ratio vs. precession, $r = 0.71$, $P < 0.001$). During a fire, charcoal fragmentation occurs along axes derived from the anatomical structure of plant species. The elongation degree is preserved even when the particle is broken (24). Experimental analysis conducted on burned grasses and wood from North America showed that charcoal from grasses has a greater elongation ratio than charcoal derived from wood (24). We thus infer that the increase in the mean elongation of microcharcoal particles is an indicator of low-intensity fires spreading in grass-dominated fueled environments. An input of microcharcoal from fynbos fires is negligible, owing to the absence of a clear correspondence between increased biomass burning and Restionaceae pollen percentages (mainly found in fynbos) from the close core GeoB1711 in the Atlantic Ocean (25) (Fig. S3).

We observed a tight correlation between the amplitude of biomass burning and the magnitude of precession changes, with high fire activity (Fig. 2*F*) occurring during precession maxima (Fig. 2*H*) and high northern hemisphere ice volume (Fig. 2*G*) (i.e., when global average temperature was cold). At those times, sea surface temperatures from southeastern Atlantic and southwestern Indian oceans were low (26, 27). Spectral analysis applied on CCnb showed a significant periodicity of 23,000 y (Fig. S4). Precession and CCnb were positively correlated ($r = 0.75$, $P < 0.001$), and precession alone accounted for 57% (adjusted R^2) of the total variance of CCnb. Fire activity changes at Wonderkrater (28), a peat bog record located within the savanna biome of eastern south Africa, where grasslands have been present throughout the last 300,000 y (29), also showed two peaks coinciding with precession maxima during the last 30,000 y, with the oldest one lagging 3,000 y precession (Fig. 2*F*). This reinforces our interpretation of a strong dependence between grass-fueled fires and precession changes.

We also observe a significant correlation ($r = 0.76$, $P < 0.001$) between biomass burning and austral summer (DJFM months) insolation at 25°S, the core's latitude (Fig. 2*I*). Our record is in phase with records of the South African monsoon (30, 31) and in opposition to the East African monsoon model (Fig. 2*J*) that responds quasi-directly to northern-hemisphere summer insolation (32). An increase in solar radiation during the southern-hemisphere summer reinforces the convection associated with the ITCZ, which in turn causes higher summer rainfall over southern Africa (30). We infer that summer rainfall accumulation at orbital timescales promotes grass fires in southern Africa (Fig. 3, *Left*). Four peaks of biomass burning fall within periods of *Podocarpus* pollen percentage increases recorded in the Indian Ocean core MD96-2048 (25) (Fig. S3). *Podocarpus* forest expansions are interpreted as indicators of humid periods in southeastern Africa (25) and are in accordance with increased summer rainfall accumulations during precession maxima. This configuration also implies the occurrence of particularly marked

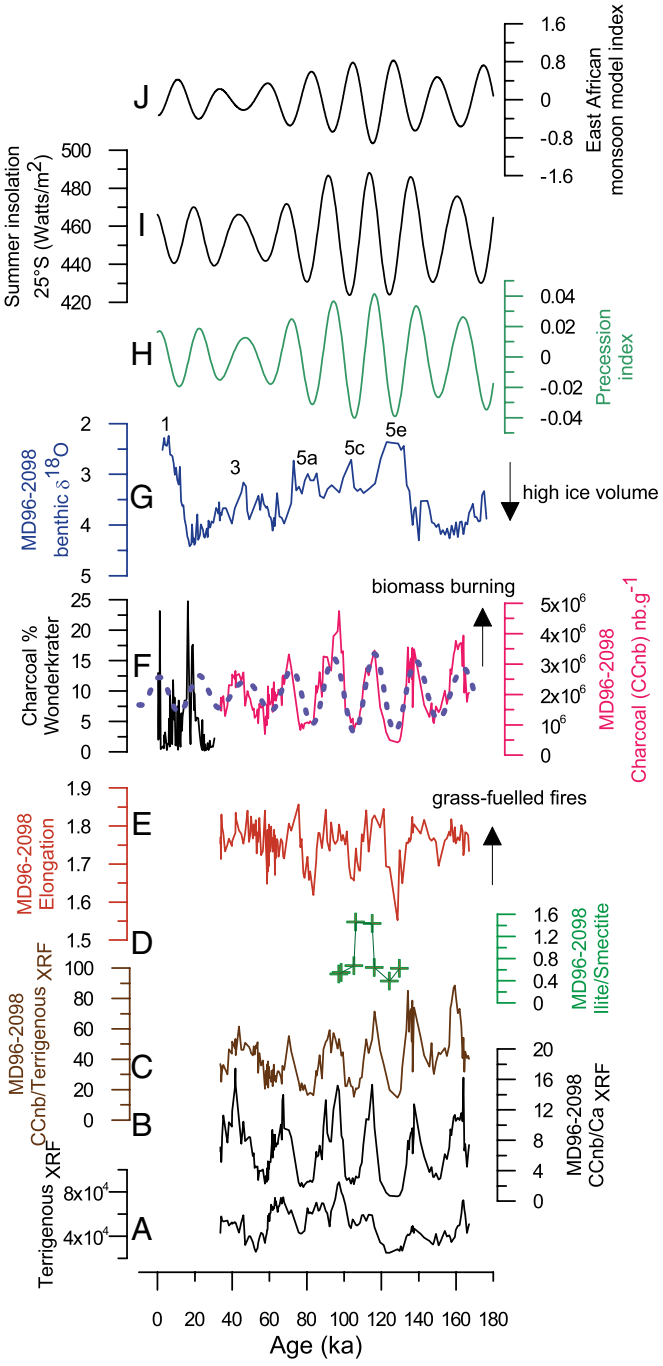

Fig. 2. Biomass burning variability of southern Africa over the last 170 ka. (*A*) Terrigenous fraction (Al+K+Ti+Fe) obtained from XRF core scanner from core MD96-2098. (*B*) Standardized microcharcoal concentration (CCnb curve) to Ca_{XRF} from core MD96-2098. (*C*) Standardized microcharcoal concentration (CCnb) to $Terrigenous_{XRF}$ from core MD96-2098. (*D*) Illite/smectite ratio from MD96-2098 clay analysis. (*E*) Elongation (ratio length/width) of microcharcoal particles. (*F*) Microcharcoal concentration curve (red) (CCnb, biomass burning); predicted biomass burning obtained from a simple linear regression model (dashed purple curve); charcoal percentage, ratios of charcoal number to all other organic particles curve from Wonderkrater peat bog (black curve) (28), age model from ref. 49 and the Abrupt Climate Changes and Environmental Responses (ACER) International Focus Group (International Union for Quaternary Science). (*G*) Benthic foraminifera oxygen isotopic curve from MD96-2098 (36). (*H*) Precession index calculated with analyseries software (47) following ref. 46. (*I*) Summer insolation (DJFM months) calculated at 25°S following ref. 46. (*J*) East African monsoon model index after ref. 32. Warm substages of Marine Isotopic Stage 5 are also indicated.

rainfall seasonality (11), the ideal situation for increasing fuel load, flammability, and fires.

Local charcoal percentage maxima during glacial isotopic stages 2, 3, 4, 5b, 5d, and 6 occur in a northern core from the eastern equatorial Atlantic (RC24-07) (33), although the peak amplitudes vary and do not match those of the precession index. Verardo and Ruddiman (33) did not interpret their data as an indicator of biomass burning, however, because levels of charcoal were low during interglacials and high during glacial periods. These results were counterintuitive because warm temperatures are associated with increased woody biomass productivity in these systems and thus increased available biomass for burning. Consequently, burning and charcoal levels were presumed to be low during glacials and high during interglacials. As a result, the authors argued that terrestrial charcoal production and ocean burial were decoupled and that the charcoal variations indicated shifts in wind strength or direction from interglacials to glacials. We propose here an alternative interpretation of the charcoal data in core RC24-07 and suggest in particular that (*i*) in addition to wooded-fuel fires, grass-fueled biomass burning is an important source of charcoal, and (*ii*) the maxima reflect increased biomass burning from grass fires during cooler climate conditions.

Our results also have implications for anthropogenic burning in Africa. Archibald et al. (34), ignoring climatic changes in their model, predict a peak in fire between 40 and 4 ky in Africa and suggest that this results from human-induced fire activity in closed/dissected landscapes. However, our data show a reduction of fire activity between 40 and 30 ky cal BP (Fig. 2*F*) that mimics the precession decrease, implying that climate was overriding any human impacts on fire at that time at least in southern Africa.

Finally, the close correspondence between the elongation ratio of microcharcoal and climate changes associated with precession suggests that charcoal morphology measurements may provide a valuable source of information about biome shifts over time, although careful parallel analyses are required to ensure that variations are not caused by transportation and deposition processes that can also have an influence on marine records. Whether these changes are due to shifts in grassland extent or productivity remains uncertain, but the latter is most likely. Dupont et al. (25) showed that the distribution of the three main biomes in southern Africa (grassland in the east and desert/semidesert in the western part) was not dictated by precession changes. We also know that rainfall can strongly affect grass biomass at one spot and that changes in rainfall (on the order of 200 mm according to ref. 30) could easily double grass productivity from ~1,000 kg/ha to ~2,000 kg/ha (35). Our elongation index therefore most likely indicates increased biomass of grassy vegetation in the eastern part of southern Africa during precession maxima.

In summary, there were six cycles of shifts in grassland and increased burning in southern Africa during the past 170,000 y. The grassland and fire cycles result from precession-driven changes in the seasonality and amount of rainfall associated with shifts in the ITCZ. During past warm periods, fire activity is reduced in southern Africa owing to an increase in summer dryness and a probable decline in grassland biomass (Fig. 3, *Right*). Our work has important implications for our understanding of fire–climate relationships, the prediction of future fire activity, the global carbon cycle, and landscape management for a region recognized as a biodiversity and climate-change hotspot (Fig. 2*F*, predicted fire curve): the current natural trend of decreasing precession is likely to result in a long-term reduction of fire activity in southern Africa due to reduced rainfall and grassland productivity. Contemporary human activities associated with landscape fragmentation and loss of vegetation connectivity may amplify this natural trend in fire reduction.

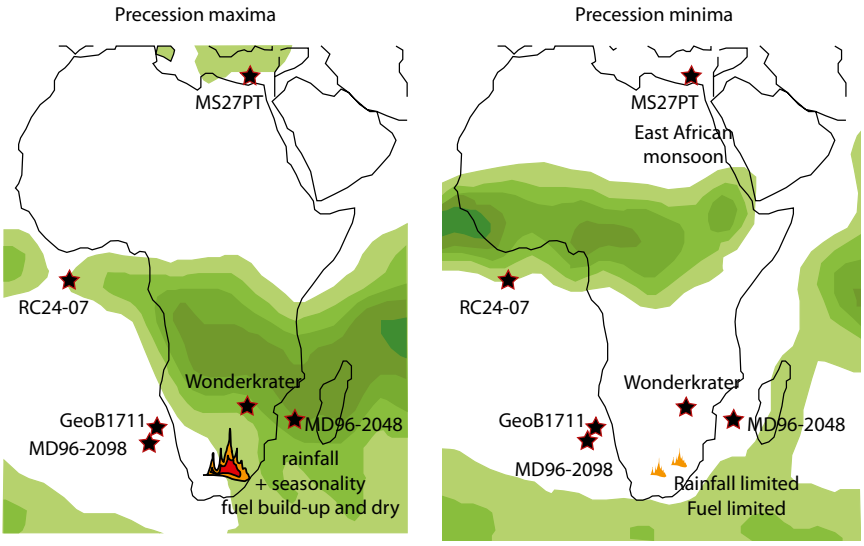

Fig. 3. Hypothesized scenarios of annual rainfall and high fire activity during precession maxima (positive values of precession index; *Left*) and annual rainfall and low fire activity during precession minima (negative values of precession index; *Right*) (Fig. 2*H*). Green shaded areas indicates rainfall amount with darker ones reflecting heavier rainfall. High rainfall in southern Africa during the precessional maxima scenario is illustrated by average austral summer (January) precipitation over 1979–1995; low rainfall in southern Africa during the precession minima scenario is illustrated by average austral winter (July) precipitation over the same period. Changes in the ITCZ are identified by the position of the most intense rainfall. Data were retrieved from the International Research Institute for Climate Prediction (http://iri.ldeo.columbia.edu). Location of cores discussed in the text.

Materials and Methods

The marine sediment core MD96-2098 (25°35′S, 12°38′E, 2,909 m water depth) was retrieved during the 1996 IMAGES II-Nausicaa cruise on the Lüderitz lower slope of the Namibian margin, north of the Orange River mouth (Fig. 1). The sediment consists of lithologically homogenous light gray to olive gray nanno- and foram-ooze with variable amounts of biogenic silica and organic matter. The chronology of the core is established by nine ^{14}C AMS (accelerator mass spectrometry) dates on planktonic foraminifera and the marine isotope stratigraphy on benthic foraminifera *Cibicioides wuellerstorfi* (36) (Table S1). ^{14}C AMS were calibrated according to the Calib6.0 radiocarbon calibration program (http://calib.qub.ac.uk/calib/) using the MARINE09.14c calibration curve and a local reservoir correction, ΔR of 157 $\pm$ 59 calculated as a mean of nine local reservoir error (ΔR for the MD96-2098 core location is available at http://calib.qub.ac.uk/marine/) (37, 38). On the basis of this chronology, the core covers the past 170,000–30,000 y.

To reconstruct biomass burning, we examined microcharcoal (average length 4–200 μm) in the sediment, which consists of small carbonized particles produced during vegetation fires. The microcharcoal extraction technique follows (39, 40), slightly modified to remove the large amount of diatoms preserved in core MD96-2098, which interferes with microcharcoal observations. A chemical treatment of 5 mL 37% hydrochloric acid (HCl), 5 mL 68% nitric acid (HNO_3), and 10 mL 33% hydrogen peroxide (H_2O_2) is performed over 24 h on approximately 0.2 g of dried sediment, followed by a chemical attack of 70% hydrofluoric acid (HF), and one HCL 25% and centrifugation to remove HF. A dilution of 0.1 is applied to the residue. The suspension is then filtered onto a membrane of 0.45 mm porosity and 47 mm in diameter. A portion of this membrane is mounted onto a slide. The particles were identified using petrographic criteria and quantified using image analysis (39, 40). Quantification of microcharcoal is performed using automated image analysis in transmitted light and following the criteria proposed by Boulter (41), who identifies charcoal as being black, opaque, and angular with sharp edges. Identification of unburned particles, characterized by the absence of plant structures and distinct level of reflectance, was used to set the best-fit threshold level to secure identification of microcharcoal by image analysis.

From measurements of microcharcoal (number, surface area, length, and width), three parameters were calculated for each sample: (*i*) the concentration of microcharcoal (CCnb) (i.e., the number of microcharcoal per gram; nb·g^{-1}); (*ii*) the concentration of microcharcoal surface (CCs), which is the sum of all surfaces of microcharcoal in one sample per gram ($\mu m^2 \cdot g^{-1}$) (using CCs avoids the overrepresentation of CCnb as the result of potential fragmentation during particle production or transport) (42); and (*iii*) the elongation of microcharcoal particles (length/width ratio). Concentrations of both abundance (CCnb) and surface area (CCs) were significantly correlated (Fig. S5), confirming that both CCnb and CCs record the same pattern of microcharcoal concentration variability. We used microcharcoal morphology (i.e., elongation) to infer the contribution of grasslands and fynbos fires to variations in microcharcoal concentrations.

To ensure that changes in microcharcoal concentrations did not reflect changes in sedimentation processes (dilution by biogenic or terrigenous material) or changes in aeolian supply, we compared CCnb with analyses of trace elements and clay mineralogy. X-ray fluorescence (XRF) analysis was performed on the surfaces of the split sediment core every 0.5 cm using a nondestructive Avaatech core-scanner (EPOC, Université Bordeaux 1). The split core surface was first covered with a 4-μm-thick Ultralene to avoid contamination of the XRF measurement unit and desiccation of the sediment. Geochemical data were obtained at different tube voltages, 10 kV for Al, K, Ca, Ti, and Fe, and 30 kV for Sr. Elemental concentrations are given as total counts (43). Eight samples were analyzed for clay mineralogy (illite, smectite, and kaolinite) at the Université de Lille 1, using X-ray diffraction following classic protocols (44). Three runs (air-dried sample, after 12 h ethylene-glycol saturation, heated at 490 °C for 2 h) were performed from 2.49° to 32.49°2θ on a Bruker D4 Endeavor set with Lynkeye fast detector, Copper anode, tube (30 kV and 30 mA). The semiquantitative estimation of the clay mineral association, based on peak characterization (45), was performed using Macintosh MacDiff4.2.5 software. Replicate samples indicate 5% error on measurements reproducibility.

We used summer insolation (DJFM months) calculated at 25°S following ref. 46 and a precession index calculated with analyseries software (47) following ref. 46 to determine how biomass burning variations were related to climate forcing.

Future long-term evolution of biomass burning in southern Africa is predicted by a simple linear regression model between CCnb and precession component over the last 170–30 ka ($r = 0.75$; $R^2 = 0.57$; $P < 0.001$). Microcharcoal data were evenly resampled using linear interpolation (step of 500 y) to match with ages of precession component. We used calculated precession from ref. 46. Then we extrapolated our observation to the last 30 ka to −10 ka (future).

ACKNOWLEDGMENTS. We thank Linda Rossignol for picking the foraminifera for carbon radiometric dating, Olivier Ther for XRF analysis, Marie-Hélène Castera and Muriel Georget for laboratory assistance, V. Hanquiez for extracting bathymetric data, Thibault Caley for providing the East African monsoon regression model data, Lydie Dupont for sharing the pollen data of

cores GeoB1711 and MD96-2048, and Louis Scott for providing Wonderkrater's charcoal data. This research was funded by European Research Council Advanced Grant TRACSYMBOLS 249587. The postdoctoral position of A.-L.D was funded by this project.

1. Bowman DMJS, et al. (2009) Fire in the Earth system. *Science* 324(5926):481–484.
2. Fischlin A, et al. (2007) Ecosystems, their properties, goods, and services. *Climate Change 2007: Impacts, Adaptation and Vulnerability. Contribution of Working Group II to the Fourth Assessment Report of the Intergovernmental Panel on Climate Change*, eds Parry ML, Canziani OF, Palutikof JP, van der Linden PJ, Hanson CE (Cambridge Univ Press, Cambridge, UK), pp 211–272.
3. Myers N, Mittermeier RA, Mittermeier CG, da Fonseca GAB, Kent J (2000) Biodiversity hotspots for conservation priorities. *Nature* 403(6772):853–858.
4. Giorgi F (2006) Climate change hot-spots. *Geophys Res Lett* 33(L08707):1–4.
5. Pechony O, Shindell DT (2010) Driving forces of global wildfires over the past millennium and the forthcoming century. *Proc Natl Acad Sci USA* 107(45): 19167–19170.
6. Liu Y, Stanturf J, Goodrick S (2010) Trends in global wildfire potential in a changing climate. *For Ecol Manage* 259(4):685–697.
7. Bradstock RA (2010) A biogeographic model of fire regimes in Australia: Current and future implications. *Glob Ecol Biogeogr* 19:145–158.
8. van der Werf GR, Randerson JT, Giglio L, Gobron N, Dolman AJ (2008) Climate controls on the variability of fires in the tropics and subtropics. *Global Biogeochem Cycles* 22(3):1–13.
9. Archibald S, Scholes RJ, Roy DP, Roberts G, Boschetti L (2010) Southern African fire regimes as revealed by remote sensing. *Int J Wildland Fire* 19:861–878.
10. Anyamba A, Justice CO, Tucker CJ, Mahoney R (2003) Seasonal to interannual variability of vegetation and fires at SAFARI 2000 sites inferred from advanced very high resolution radiometer time series data. *J Geophys Res* 108(13):8507.
11. Tyson PD, Preston-Whyte RA (2000) *The Weather and Climate of Southern Africa* (Oxford University Press Southern Africa, Cape Town, South Africa), p 396.
12. Manry DE, Knight RS (1986) Lightning density and burning frequency in South African vegetation. *Vegetatio* 66:67–76.
13. Cowling RM, Richardson DM, Pierce SM (2004) *Vegetation of Southern Africa* (Cambridge Univ Press, Cambridge, UK), pp 652.
14. Carmona-Moreno C, et al. (2005) Characterizing interranual variations in global fire calendar using data from Earth observing satellites. *Glob Change Biol* 11: 1537–1555.
15. Archibald S, Nickless A, Govender N, Scholes RJ, Lehsten V (2010) Climate and the inter-annual variability of fire in southern Africa: A meta-analysis using long-term field data and satellite-derived burnt area data. *Glob Ecol Biogeogr* 19:794–809.
16. Peucker-Ehrenbrink B (2009) Land2Sea database of river drainage basin sizes, annual water discharges, and suspended sediment fluxes. *Geochem Geophys Geosyst* 10(6): Q06014.
17. Shannon LV, Nelson G (1996) The Benguela: Large scale features and processes and system variability. *The South Atlantic Ocean, Present and Past Circulation*, eds Wefer G, Berger WH, Siedler G, Webb D (Springer, Berlin), pp 163–210.
18. Marlow JR, Lange CB, Wefer G, Rosell-Mele A (2000) Upwelling intensification as part of the Pliocene-Pleistocene climate transition. *Science* 290(5500): 2288–2291.
19. Etourneau J, Schneider R, Blanz T, Martinez P (2010) Intensification of the Walker and Hadley atmospheric circulations during the Pliocene–Pleistocene climate transition. *Earth Planet Sci Lett* 297:103–110.
20. Etourneau J, Martinez P, Blanz T, Schneider R (2009) Pliocene–Pleistocene variability of upwelling activity, productivity, and nutrient cycling in the Benguela region. *Geology* 37(10):871–874.
21. Little MG, et al. (1997) Rapid palaeoceanographic changes in the Benguela Upwelling System for the last 160,000 years as indicated by abundances of planktonic foraminifera. *Palaeogeogr Palaeoclimatol Palaeoecol* 130:135–161.
22. Bayon G, Gennan CR, Nesbitt RW, Bertrand P, Schneider RR (2003) Increased input of circumpolar deep water-borne detritus to the glacial SE Atlantic Ocean. *Geochem Geophys Geosyst* 4(3):1–13.
23. Heine K, Volkel J (2010) Soil clay minerals in Namibia and their siginificance for the terrestrial and marine past global change research. *Afr Study Monogr* 40: 31–50.
24. Umbanhowar CEJ, McGrath MJ (1998) Experimental production and analysis of microscopic charcoal from wood, leaves and grasses. *Holocene* 8:341–346.
25. Dupont L (2011) Orbital scale vegetation change in Africa. *Quat Sci Rev* 30(25-26): 3589–3602.
26. Caley T, et al. (2011) High-latitude obliquity as a dominant forcing in the Agulhas current system. *Climate of the Past* 7:1285–1296.
27. Kirst GJ, Schneider RR, Muller PJ, von Storch I, Wefer G (1999) Late quaternary temperature variability in the Benguela current system derived from alkenones. *Quat Res* 52:92–103.
28. Scott L (2002) Microscopic charcoal in sediments: Quaternary fire history of the grassland and savanna regions in South Africa. *J Quaternary Sci* 17(1):77–86.
29. Scott L (2002) Grassland development under glacial and interglacial conditions in southern Africa: Review of pollen, phytolith and isotope evidence. *Palaeogeogr Palaeoclimatol Palaeoecol* 177:47–57.
30. Partridge TC, DeMenocal PB, Lorentz SA, Paiker MJ, Vogel JC (1997) Orbital forcing of climate over South Africa: A 200,000 year rainfall record from the Pretoria Saltpan. *Quat Sci Rev* 16:1125–1133.
31. Kristen I, et al. (2007) Hydrological changes in southern Africa over the last 200 Ka as recorded in lake sediments from the Tswaing impact crater. *S Afr J Geol* 110: 311–326.
32. Caley T, et al. (2011) Orbital timing of the Indian, East Asian and African boreal monsoons and the concept of a 'global monsoon' *Quat Sci Rev* 30:3705–3715.
33. Verardo DJ, Ruddiman WF (1996) Late Pleistocene charcoal in tropical Atlantic deep-sea sediments: Climatic and geochemical significance. *Geology* 24(9):855–857.
34. Archibald S, Staver AC, Levin SA (2012) Evolution of human-driven fire regimes in Africa. *Proc Natl Acad Sci USA* 109(3):847–852.
35. Scholes RJ (1990) The influence of soil fertility on the ecology of southern African dry savannas. *J Biogeogr* 17(4/5):415–419.
36. Bertrand P, et al. (2002) Occurrence of an exceptional carbonate dissolution episode during early glacial isotope stage 6 in the Southeastern Atlantic. *Mar Geol* 180: 235–248.
37. Stuiver M, Reimer PJ (1993) Extended 14C database and revised CALIB radiocarbon calibration program. *Radiocarbon* 35:215–230.
38. Reimer PJ, et al. (2009) IntCal09 and Marine09 radiocarbon age calibration curves, 0-50,000 years cal BP. *Radiocarbon* 51(4):1111–1150.
39. Daniau A-L, et al. (2007) Dansgaard-Oeschger climatic variability revealed by fire emissions in southwestern Iberia. *Quat Sci Rev* 26:1369–1383.
40. Daniau A-L, Sánchez-Goñi MF, Duprat J (2009) Last glacial fire regime variability in western France inferred from microcharcoal preserved in core MD04-2845, Bay of Biscay. *Quat Res* 71(3):385–396.
41. Boulter MC (1994) An approach to a standard terminology for palynodebris. *Sedimentation of Organic Particles*, ed Traverse A (Cambridge Univ Press, Cambridge, UK), pp 199–216.
42. Théry-Parisot I (1998) *Economie du combustible et Paléoécologie en contexte glaciaire et périglaciaire, Paléolithique moyen et supérieur du sud de la France. Anthracologie, Experimentation, Taphonomie*. PhD thesis (Panthéon-Sorbonne Univ de Paris I, Paris).
43. Richter TO, et al. (2006) The Avaatech XRF Core Scanner: Technical description and applications to NE Atlantic sediments. *New Techniques in Sediment Core Analysis* (Geological Society Special Publication 267), ed RG Rothwell (Geological Society, London), pp 39–50.
44. Bout-Roumazeilles V, Debrabant P, Labeyrie L, Chamley H, Cortijo E (1997) Latitudinal control of astronomical forcing parameters on the high-resolution clay mineral distribution in the 45 degrees-60 degrees N range in the North Atlantic Ocean during the past 300,000 years. *Paleoceanography* 12:671–686.
45. Bout-Roumazeilles V, Cortijo E, Labeyrie L, Debrabant P (1999) Clay mineral evidence of nepheloid layer contributions to the Heinrich layers in the northwest Atlantic. *Palaeogeogr Palaeoclimatol Palaeoecol* 146:211–228.
46. Berger A (1978) Long-term variations of daily insolation and Quaternary climatic change. *J Atmos Sci* 35:2362–2367.
47. Paillard D (1996) Macintosh Program performs time-series analysis. *Eos Trans AGU* 77(39):379.
48. White F (1983) The vegetation of Africa. *Natural Rescourses Research 20* (United Nations Educational, Scientific and Cultural Organization, Paris).
49. Scott L, Holmgren K, Talma A, Woodborne S, Vogel JC (2003) Age interpretation of the Wonderkrater spring sediments and vegetation change in the savanna biome, Limpopo Province, South Africa. *S Afr J Sci* 99:484–488.